Stochastic model for the residence time of solid particles in turbulent Rayleigh-Bénard flow

Colin J. Denzel
Department of Aerospace and Mechanical Engineering, University of Notre Dame, Notre Dame, Indiana 46556, USA

Andrew D. Bragg
Department of Civil and Environmental Engineering, Duke University, Durham, North Carolina 27708, USA

David H. Richter
Department of Civil and Environmental Engineering and Earth Sciences, University of Notre Dame, Notre Dame, Indiana 46556, USA

(Received 26 August 2022; accepted 2 February 2023; published 27 February 2023)

The Pi Chamber generates moist turbulent Rayleigh-Bénard flow in order to replicate steady-state cloud conditions. We take inspiration from this setup and consider a particle-laden, convectively driven turbulent flow using direct numerical simulation. The aim of our paper is to develop a simple stochastic model that can accurately describe the residence times of the particles in the flow, this time being determined by the complex competition between the gravitational settling of the particles, and the interaction of the particles with the turbulent structures in the flow. A simple conceptual picture underlies the stochastic model, namely that the particles take repeated trips between the top and bottom boundaries, driven by the convective cells that occur in Rayleigh-Bénard turbulence, and that their residence times are determined by the time it takes to complete one of these trips, which varies from one trip to another, and the probability of falling out to the bottom boundary after each trip. Despite the simplicity of the model, it yields quantitatively accurate predictions of the distribution of the particle residence times in the flow. We independently vary the Stokes numbers and settling velocities in order to shed light on the independent roles that gravity and inertia play in governing these residence times.

DOI: 10.1103/PhysRevFluids.8.024307

I. INTRODUCTION

The settling of inertial particles in turbulent flows is relevant to a wide array of engineered and natural systems, including the dispersion of pollutants [1], the settling of organic materials in the ocean [2], and the cooling of Earth's magma [3]. In this paper we are particularly motivated by experiments conducted in the so-called Pi Chamber, a cloud chamber facility located at Michigan Technological University which uses two temperature-controlled, saturated plates in order to replicate cloud conditions via moist turbulent Rayleigh-Bénard (RB) flow. The chamber itself has been described extensively elsewhere [4], including efforts to characterize unladen RB flow in moist conditions [5], and for this paper it serves as a broad motivation for understanding the Lagrangian dynamics of particles, especially their gravitational sedimentation. To this end, the Pi Chamber will serve as the starting point, although our exploration will extend beyond the properties of the particles seen in the experimental facility itself; i.e., our analysis spans ranges of nondimensional parameters

that cannot be replicated experimentally in order to gain further insight into the separate roles of gravity and inertia on the particle residence times in the flow.

Existing studies on particle laden RB turbulence have largely focused on how thermal and dynamic coupling affects turbulence and particle motion, primarily via two-way coupled simulations that attempt to take into account all of the physics relevant to the onset of turbulence and the transfer of heat and momentum [6–8]. In a somewhat similar setup to the Pi Chamber, Oresta and Prosperetti [9] simulated RB flow and allowed solid, isothermal particles to settle from the top boundary. Over a wide range of particle diameters, they found that mechanical and thermal coupling were able to change the mean particle settling velocities. The results also suggested a tendency towards "reverse one-way coupling" where varying fluid parameters had a small effect on the behavior of the particles. In light of this, we are interested in particle residence times as a function of particle properties and will only consider one set of flow parameters, with the understanding that for a sufficiently turbulent environment, all of the relevant mechanisms will be present.

The study of isothermal, inertial particles was furthered in Yang *et al.* [10], which considered particles with three different Stokes numbers (St). They found that both heat and momentum transfer were significantly enhanced for the medium Stokes number due to strong coupling of the two phases, while the coupling for the lowest and highest St was weak. This nonmonotonic relationship between particle dispersion and St has been frequently observed in other particle-laden turbulent flows [11]. In an effort to isolate the effects of inertia from gravitational forces in turbulent, two-way coupled RB flow, Park *et al.* [12] looked at nonisothermal particles and varied St and a scaled settling velocity (V_s) independently, allowing for a more detailed exploration of momentum coupling. Although this study [12] was more focused on how thermal and mechanical coupling changed the turbulent kinetic energy and Nusselt number of the flow, the approach of independently varying St and V_s is an essential component of the current paper.

The discussion of settling rates and residence times of small heavy particles is a well-studied aspect of turbulent flows in general. Historically, these efforts have been focused on isotropic, homogeneous turbulence with zero mean velocity. It has been demonstrated that the settling of these particles is dependent on the particle inertia and the free-fall terminal velocity. When there is no inertia, the particles on average settle at the same rate as in still fluid. However, inertia can create a bias for particles to move towards downwards-sweeping regions of the flow [13]. The resulting mechanics have since been studied extensively [14–16], showing that inertial clustering and gravitational settling lead to preferential sweeping and ultimately increased settling velocities when compared to the velocity predicted by Stokes drag in a quiescent medium. In Rosa *et al.* [17], where it was shown that preferential sweeping was the dominant means of increasing average settling velocity, the inertial and gravitational settling parameters were separated by varying the ratio of particle to fluid density and the energy dissipation rate. Furthermore, another mechanism proposed in [17] is called loitering, which refers to falling particles spending more time in regions with upward flow, ultimately reducing average settling velocities. In numerical simulations of homogeneous isotropic turbulence, this mechanism only plays a role when nonlinear drag is considered [18], which is not used in the present simulations.

In the present setup, we also must account for the effects of boundary layers near the wall. The settling velocities of inertial particles through wall-bounded turbulence were studied in Bragg *et al.* [19,20], which explored theoretically the physical mechanisms governing the particle transport, and used direct numerical simulation (DNS) to explore how the various mechanisms contribute as V_s and St are varied. While it was evident that the well-known effects of preferential sweeping were present in the bulk of the flow, the contribution of this mechanism decreased near the wall. In the near-wall region where the gradients in the turbulence statistics are strong, the turbophoretic drift mechanism [21] takes over and becomes the dominant mechanism responsible for the enhanced settling speed of the particles. This is in fact the same mechanism that is also responsible for a buildup of the particle concentration near the wall even in the absence of settling [21]. These additional considerations complicate the problem and have led to the implementation of stochastic models of varying complexity [22–24].

Understanding and modeling particle settling rates and residence times are relevant to understanding the formation of cloud droplets in the Pi Chamber. Works such as Chandrakar and Yang [25] have studied the droplet size distributions (DSDs) in experimental clouds by deriving analytical solutions to the Fokker-Planck equations given various turbulence and droplet removal assumptions. Similarly, in Saito *et al.* [23], the focus was on the development of a Fokker-Planck equation and its prediction of the broadening of DSD. In order to facilitate the comparison with statistical theory, they took the simplest approach by assuming that the removal process (and therefore droplet lifetime) was independent of particle size. In a similar exploration of an evolving Pi Chamber DSD, Krueger [22] assumed that when a droplet becomes sufficiently close to the lower boundary, the probability of falling out per unit time is determined by the terminal velocity, which is assumed to follow Stokes law and is therefore proportional to the square of the radius. In this paper, we show that these assumptions [22,23] are valid, but only within certain regimes of St and V_s. Our proposed model accounts for the relevance of the Bénard cells and allows us to separate the effects of inertia and gravitational forces. This is achieved through a small number of parameters relevant to RB flow that are dependent on St and V_s. We will demonstrate how these parameters vary with particle properties, and how these variations ultimately determine residence times.

II. METHODS

A. Numerical setup

To generate statistical data for the development of our stochastic model, we employ a DNS of the turbulent Rayleigh-Bénard flow. The resulting flow is then one-way coupled with Lagrangian particles, meaning that while the fluid is able to impart momentum to the particles, the particles do not modify the background flow. As noted above, the setup is broadly motivated by the conditions found in the Pi Chamber, and therefore is similar to the methods used by MacMillan *et al.* [26], except that in the present case the particles are nonevaporating and one-way coupled to the surrounding flow. While we will provide a brief overview of the DNS model as it pertains to this paper, further details can be found in Richter *et al.* [27], Park *et al.* [12], and Helgans and Richter [28].

The Navier-Stokes equations with the Boussinesq approximation are solved for mass, momentum, and energy conservation of the carrier phase:

$$\nabla \cdot \mathbf{u} = 0, \tag{1}$$

$$\frac{\partial \mathbf{u}}{\partial t} + \mathbf{u} \cdot \nabla \mathbf{u} = -\nabla \pi + \hat{\mathbf{k}} \frac{g}{T_0} T + \nu \nabla^2 \mathbf{u}, \tag{2}$$

$$\frac{\partial T}{\partial t} + \mathbf{u} \cdot \nabla T = \alpha \nabla^2 T, \tag{3}$$

where $\mathbf{u}$ is the fluid velocity, T is the temperature, and π is a pressure variable which enforces the divergence-free condition of Eq. (1). In Eq. (2), the buoyancy term in the vertical direction is dependent on the acceleration due to gravity $\mathbf{g} = g\hat{\mathbf{k}}$, and the reference temperature $T_0 = 300$ K. The terms ν and α refer to the kinematic viscosity and heat diffusivity of the fluid. Since we are considering solid, one-way coupled particles, there is no need for the additional source terms from particle coupling that are found in MacMillan *et al.* [26] and Park *et al.* [12]; this will allow us to vary the gravity felt by each particle in later analysis without concern for the effects that the particles may have on one another or the flow.

Along the upper and lower boundaries, the fluid velocity is governed by a no slip condition. The aspect ratio of the domain is $L_x/L_z = L_y/L_z = 2$, and the number of grid points is $[N_x, N_y, N_z] = [128, 128, 128]$. The 2:1 aspect ratio is similar to that found in the Pi Chamber. However, unlike the Pi Chamber, the domain is horizontally periodic owing to the pseudospectral discretization in the x and y directions. Second order finite differences are employed for derivatives in the vertical z direction. The temperatures of the upper and lower boundaries of the rectangular domain are set to

$T_{\text{top}} = 280$ K and $T_{\text{bot}} = 299$ K, resulting in a temperature difference $\Delta T = 19$ K. This corresponds to a Rayleigh number of $\text{Ra} \equiv (g\Delta T L_z^3)/(T_0 \nu\alpha) = 10^7$. This value is used for all simulations in this paper, along with a Prandtl number $\text{Pr} \equiv \nu/\alpha = 0.715$.

The particles evolve in a Lagrangian frame of reference according to the following set of equations:

$$\frac{d\mathbf{x}_p^i}{dt} = \mathbf{v}_p^i, \tag{4}$$

$$\frac{d\mathbf{v}_p^i}{dt} = \frac{1}{\tau_p}\left(\mathbf{u}_f - \mathbf{v}_p^i\right) - g_p\hat{\mathbf{k}}, \tag{5}$$

where the evolutions of the ith particle's position $\mathbf{x}_p^i$ and velocity $\mathbf{v}_p^i$ depends solely on τ_p, g_p, and the local fluid velocity $\mathbf{u}_f$ interpolated to the droplet location using trilinear interpolation. All particles begin their lifetime at the midplane with zero initial velocity and are taken out of the flow when they reach the bottom boundary. It is worth noting that, for simplicity, Eq. (5) neglects terms from the full Maxey-Riley equations [29]. As will be evident in later sections, the model uses statistics taken directly from the DNS. Therefore, while these additional terms may result in some quantitative changes to the probability density functions (PDFs), any additional physics captured in the simulation could straightforwardly be accounted for without any changes to the model.

The timescale $\tau_p = \rho_a d^2/18\nu\rho_f$ is the Stokes timescale, which governs the time taken by a particle of diameter d to reach equilibrium with the local velocity of a fluid that has density ρ_f and kinematic viscosity ν. The gravitational acceleration experienced by the particle, g_p, is separate from that experienced by the fluid g, thus allowing us to specify the particle settling rate independent of the buoyancy forcing of the fluid. Using Kolmogorov microscales to nondimensionalize the velocities in Eq. (5), we obtain the following:

$$\text{St}\frac{d\tilde{\mathbf{v}}_p^i}{d\tilde{t}_k} = \left(\tilde{\mathbf{u}}_f - \tilde{\mathbf{v}}_p^i\right) - V_s\,\hat{\mathbf{k}}. \tag{6}$$

As a result, it is evident that particle motion is solely dependent on two nondimensional parameters: St and V_s. For the purposes of this paper, they will be defined as $\text{St} = \tau_p/\tau_k$ and $V_s = \tau_p g_p/v_k$ where τ_k and v_k are the vertically averaged Kolmogorov time and velocity microscales, respectively. Note that the nondimensional time $\tilde{t}_k = t/\tau_K$ is used in Eq. (6) to define St and V_s. A separate time scale that will be used extensively in this paper is a convective time scale defined as $\tilde{t}_c = t/\tau_e$. The parameter τ_e is the eddy turnover time given by $\tau_e = 2L_z/\sqrt{\langle u_z^2\rangle_{V,t}}$, where $\langle\rangle_{V,t}$ indicates a volumetric and temporal mean of the vertical velocity (u_z) squared, a turnover time definition used in multiple works by Sakievich [30,31]. For this simulation, $\tau_e = 3.95$ min; how this relates to predicting particle residence times will be explored in a later section.

Unladen RB flow has been studied extensively in the literature [32], and therefore will not be a focus of discussion in this paper. More details on the specific setup used to inspire and generate the flow in this application can be found in Chang *et al.* [4] and MacMillan *et al.* [26]. The focus for the remainder of this paper will be on understanding and modeling the lifetime behavior of solid, one-way coupled particles as a function of St and V_s.

B. Model description

The processes and mechanisms that govern particle transport in turbulent Rayleigh-Bénard flow are very complicated. However, the conceptual framework behind our model assumes that a relatively small number of flow quantities and simple processes determine the probability distribution of the particle residence times. This conceptual framework is inspired by the observation that particles are circulated globally by the convection cells in the flow, causing them to take a number of "elevator trips" before eventually falling out; the number of these trips largely influences the total residence time.

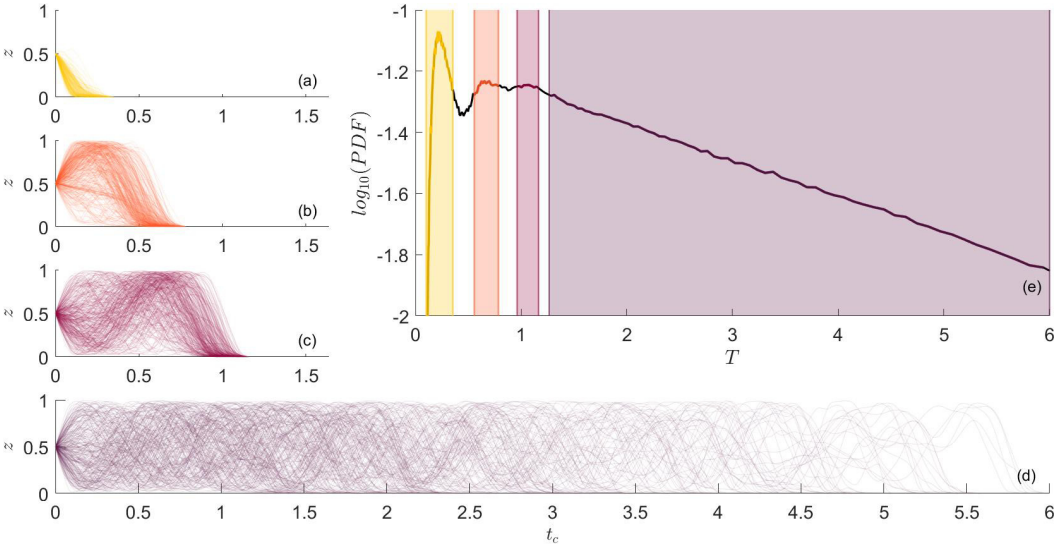

FIG. 1. Sample distribution of the nondimensional residence times (T) as defined in Eq. (7), resulting from the DNS (e). To emphasize the importance of elevator trips on the qualitative nature of the distribution, see the trajectories from the first (a), second (b), and third (c) peaks, as well as the tail of the distribution (d).

Concerning the dependence of the particle dynamics on St and V_s, a couple of limiting cases have straightforward interpretations. In the limit of zero inertia and terminal velocity, i.e., $V_s \to 0$ and $\mathrm{St} \to 0$, the particles will act as fluid tracers. These are continuously circulated by the convection with no chance of falling out in finite time because we do not consider diffusive processes. In contrast, as $V_s \to \infty$ and $\mathrm{St} \to \infty$ the infinite inertia eliminates the effect of the flow and prevents the particle from ever accelerating to its terminal velocity. Another frequently made simplification assumes that $V_s \approx$ finite and $\mathrm{St} \to 0$. In this case, for particles that are initially distributed homogeneously, the mean velocity of the particles would be the Stokes settling velocity because their lack of inertia means that the particles sample the flow uniformly for all times. This is the assumption behind the well-known Rouse profile of suspended particulate matter [33]. In the majority of applications, however, including the droplets found in the Pi Chamber, the presence of a finite nonzero St introduces the complicating role of inertia.

The elevator trips that inspire this model are highlighted in Fig. 1, which shows a sample probability distribution of particle residence times from the DNS nondimensionalized by τ_e [Fig. 1(e)], and identifies with color shading representative trajectories that correspond to its most obvious features. If the trajectories were approximated to be sinusoidal, we could consider one of these elevator trips to be one period that begins and ends at the midplane. The first two peaks in the distribution are a result of those that either had an initial downward velocity and only traversed the distance from midplane to bottom boundary, or those that had an initial upward velocity and completed one-half period before traversing the same final distance. The remaining particles then complete an unspecified number of elevator trips before ultimately traversing the distance from the midplane to the bottom boundary. It is then evident that, in order to approximate the residence time of a particle, we need four pieces of information: (1) (λ_d) how likely the particle is to have an initial downward velocity, (2) (ρ_e) the amount of time it takes the particle to complete one elevator trip, (3) (λ_f) how likely the particle is to fall out of the flow after each trip, and (4) (ρ_b) how much time it takes the particle to traverse from the midplane to the bottom boundary before falling out.

These are the four parameters that the stochastic model takes into account to predict the full distribution of residence times, and are expected to be a function of both St and V_s. Our goal is to

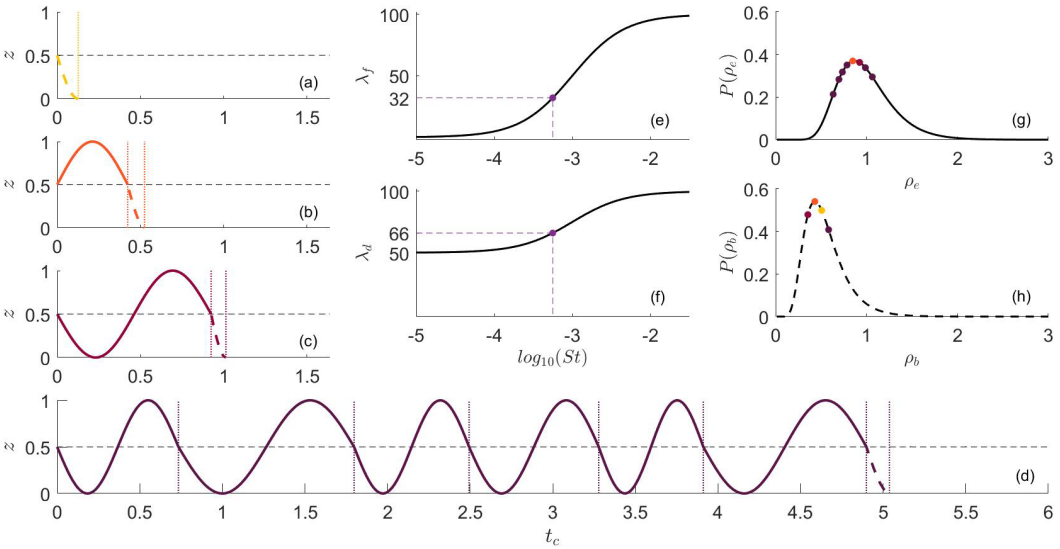

FIG. 2. Demonstration of the stochastic model for four trajectories given particles of the same size, where $\{\xi = -1,\ N_t = 0\}$ (a), $\{\xi = 1,\ N_t = 0\}$ (b), $\{\xi = -1,\ N_t = 1\}$ (c), and $\{\xi = -1,\ N_t = 6\}$ (d). The residence time predictions take into account the chance of falling out after each elevator trip, λ_f (e), the likelihood of having an initial downward velocity, λ_d (f), the time required to complete an elevator trip (as defined in the "Model description" section), ρ_e, denoted by solid lines (g), and the time to traverse from the midplane to the bottom boundary, ρ_b, denoted by dashed lines (h).

demonstrate this dependence in the formulation of this model. For the remainder of this paper, the reported values of ρ_e and ρ_b will be nondimensionalized by the eddy turnover time τ_e.

In order to construct a stochastic model based on this conceptual framework, two steps are required to determine the residence time of the ith particle, T_i.

(1) Determine whether the particle has an initial upward or downward velocity based on λ_d. While no additional considerations must be taken for an initial downward velocity, if it is upward, add the time associated with half of an elevator trip ($\rho_e/2$).

(2) Determine if the particle will fall out of the flow based on λ_f. If it does, add the time required to pass from the midplane to bottom boundary ρ_b and consider the particle dead. If the particle does *not* fall out, add the time required for an elevator trip ρ_e, and repeat step 2 until the particle does fall out of the flow.

How this simple process replicates the trajectories shown in Fig. 1 is demonstrated visually in Fig. 2. In Figs. 2(a) and 2(b), we see particles that complete zero elevator trips and have initial downward and upwards velocities respectively. Figure 2(c) shows a particle completing one elevator trip before falling out, while Fig. 2(d) shows a particle completing multiple elevator trips.

The procedure described above may be summarized mathematically as follows. Let ξ denote a random variable living in a discrete sample space that takes values -1 and $+1$, with probability $\mathbb{P}(\xi = -1) = \lambda_d$, and hence $\mathbb{P}(\xi = +1) = 1 - \lambda_d$. The configuration $\xi = -1$ is used to denote that the initial particle velocity is down, while $\xi = +1$ denotes that it is up. The nondimensional residence time for the ith particle, T_i, is then specified by the model to be

$$T_i = \sum_{j=0}^{N_t} \beta(j, \xi)\rho_e^{(j)} + \rho_b \tag{7}$$

where $\beta(j = 0, \xi = -1) = 0$, $\beta(j = 0, \xi = +1) = 1/2$, and $\beta(j, \xi) = 1\ \forall j > 0, \xi$, with N_t being the total number of elevator trips taken by the particle before it falls out. The quantity $\rho_e^{(j)}$ simply

denotes the value of ρ_e at the jth step of the iteration. It is worth emphasizing that the values of ρ_e and ρ_b are drawn from the full distribution obtained in the DNS. While the use of mean values would be simpler, it would prevent us from replicating the full residence PDF, as there would only be residence times at integer multiples of $\overline{\rho_e}$.

In order for this new model to be fully closed and predictive, the statistical quantities summarized above would have to be modeled. However, as a first step we simply specify them using the DNS data. The advantage of doing this is that it allows the simple conceptual idea underlying the stochastic model to be tested. We intend to show that, given full knowledge of these few essential parameters, the framework is sufficient to replicate the DNS results. Given the complexity of particle motion in turbulent Rayleigh-Bénard flow, it is not at all obvious *a priori* that our simple conceptual framework is sufficiently detailed to quantitatively capture the particle residence times in the flow. Once the accuracy of this conceptual modeling framework has been established, it will then make sense to try to model the input statistics and so derive a fully closed, fully predictive model. While there is some discussion of potential simplifying assumptions in the conclusion, the development of a fully closed model is left to future work.

III. RESULTS

Here we discuss the particle residence time behavior observed in the DNS, as well as the performance of the model as St and V_s are varied. The varying of St and V_s follows two different strategies. In the first, V_s and St are inherently coupled, as they would be in a physical experiment where the acceleration of gravity felt by the particles g_p would equal that responsible for the buoyancy forcing g. While this is consistent with physical experiments, it does not allow for the effects of gravity and inertia to be untangled, which can hinder an understanding of the problem. To explore this, we therefore also consider cases where V_s is held constant (by varying g_p) while varying St, allowing us to distinguish the effects of gravitational settling from particle inertia on the particle residence times.

A. Coupled St and V_s

For the coupled case, we consider particles with a range of Stokes numbers $\mathrm{St} = [10^{-6}, 10^{-1}]$, which, since the flow and particles experience the same gravitational acceleration, implies the range $V_s = [10^{-3}, 10^{2}]$. For reference, a 0.5 micron salt aerosol in the Pi Chamber has $\mathrm{St} \sim \mathcal{O}(10^{-6})$ and $V_s \sim \mathcal{O}(10^{-3})$, and a 20 micron cloud water droplet has $\mathrm{St} \sim \mathcal{O}(10^{-3})$ and $V_s \sim \mathcal{O}(10^{0})$. While our range encompasses realistic values, we are also intentionally considering a wider range in order to more comprehensively understand the problem and test the model.

The four statistical quantities required for the model are shown in Fig. 3, as measured by the DNS and used in the model results of Figs. 4 and 5. For both distributions, a discrete PDF is generated directly from the DNS data and then fit with cubic splines in order to create a continuous cumulative distribution function (CDF). The model then uses inverse transform sampling by pulling from this CDF to generate pseudorandom numbers that adhere to the probability distribution of our choice. The PDF of period residence times, $P(\rho_e)$, seen in Fig. 3(a), clearly shows that for this range of properties, the majority of particles complete an elevator trip in accordance with the convective time (t_c). Note that there are no data for the largest St, as at this size no particles completed an elevator trip. The distribution of times for a particle to traverse from the midplane to the bottom boundary, $P(\rho_b)$, seen in Fig. 3(b), however, is strongly correlated with St, with smaller times being associated with larger particles. This is because the increased settling velocity and inertia of the particles lead to a larger terminal velocity and increasingly negligible effects of the flow. The chance of having an initial downward velocity, λ_d, is approximately 50% for the smaller St, but rises to 100% for the largest. Since there is no mean vertical fluid velocity at the midplane, we would expect minimally inertial particles initialized there (with no initial velocity) to have an equal chance of being carried up or down. Similarly, the percent chance of falling out during an elevator trip, λ_f, starts below 10%

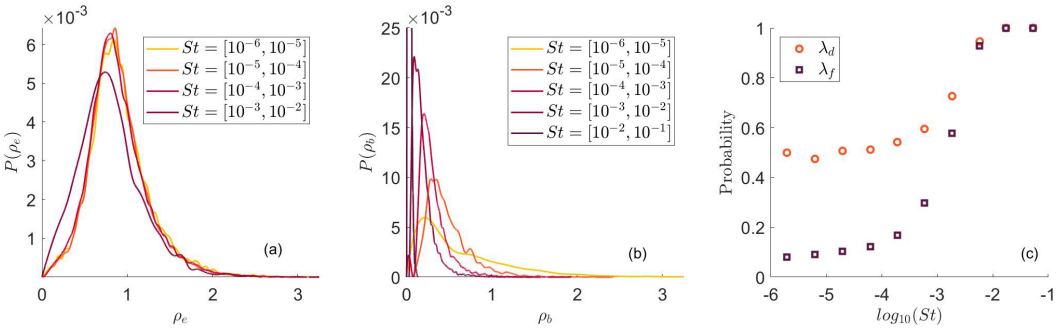

FIG. 3. The four input parameters from the coupled St and V_s case: the distribution of elevator trips as defined in the model description, ρ_e (a), the distribution of the time to pass from the midplane to bottom boundary, ρ_b (b), as well as the chance of an initial downward velocity, λ_d, and the chance of falling out after an elevator trip, λ_f (c), expressed as probabilities.

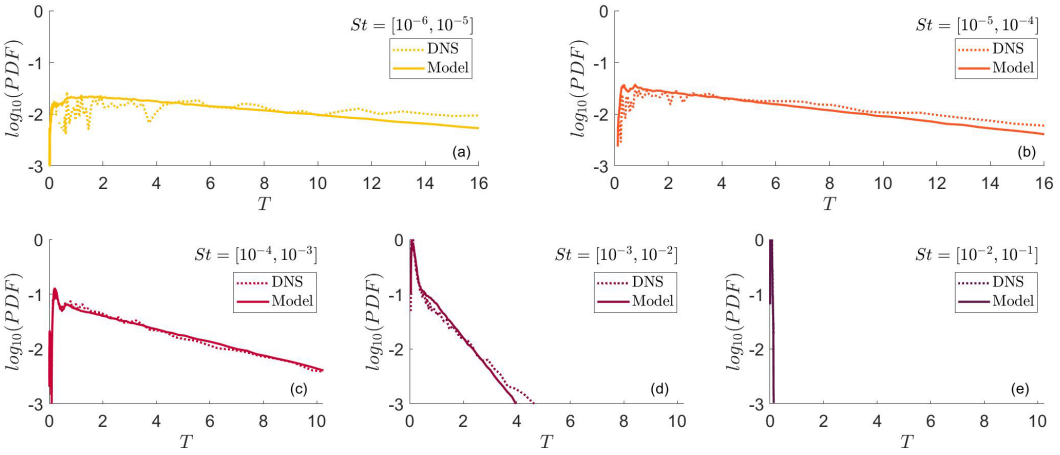

FIG. 4. For each order of magnitude considered in the coupled St and V_s case [(a)–(e)], the model has been tested by comparing the full distributions of nondimensional residence times (T) to the DNS results.

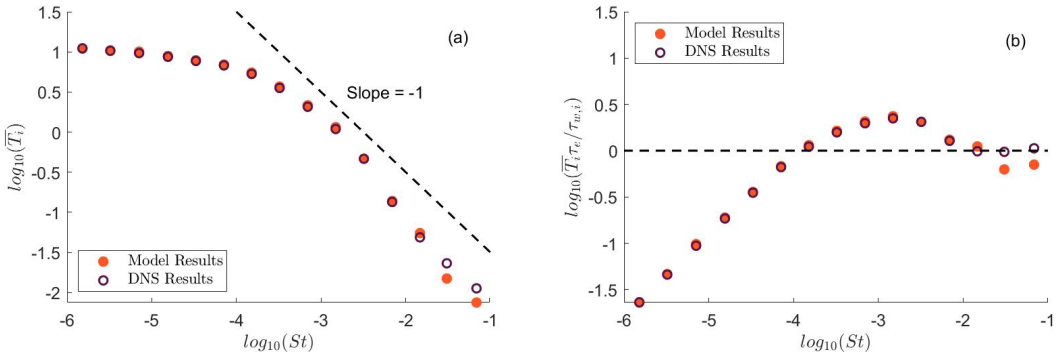

FIG. 5. The results of the coupled St and V_s case as shown by the comparison of mean nondimensional residence times ($\overline{T_i}$), with a reference slope included for comparison to the power law relationship predicted by Stokes drag (a). The same results are also plotted where the mean residence time is instead nondimensionalized by the settling time of a given particle in quiescent flow ($\tau_{w,i}$) (b).

but rises to 100% for the larger St, meaning all particles of that size are unable to complete a full elevator trip due to their inertia and gravitational settling..

With these four inputs, Fig. 4 compares the PDFs of residence times as measured in the DNS to those generated by the model. Figure 5 compares the mean residence times predicted by DNS and the model as a function of St. We see that the model captures nearly all relevant features of the DNS PDF, including the peaks at low t_c, and is quantitatively accurate for all ranges of St. Unsurprisingly, we see that the larger particles, those with both high St and V_s values, on average fall out faster than their smaller counterparts. Recalling that the residence times in Figs. 4 and 5(a) have been normalized by the convective time scale of the flow, we see the two expected peaks around $1/4$ and $3/4$ periods. Beyond those peaks, the linear nature of the log-scale PDFs suggests qualitative agreement with the results of Patočka *et al.* [3], who demonstrated that the number of suspended particles in a system could be robustly modeled with an exponential decay relationship dependent on the settling velocity and flow properties. In Fig. 5, we see that for $\mathrm{St} < 10^{-4}$, the particles all take an average of ten elevator trips before falling out. In this regime, the assumption made in Saito *et al.* [23] that lifetime is independent of particle properties may be sufficient. It appears that the trajectory is dominated by convection, and the slight nonzero slope is only caused by the different distributions of ρ_b (as ρ_e, λ_d, and λ_f remain largely unchanged). These results are qualitatively similar to what was seen by Patočka *et al.* [3], which also identified a regime of slow sedimentation dominated by large-scale circulation. The number of trips continues to decrease, until beyond $\mathrm{St} = 10^{-3}$ we see that the residence time is on average less than one convective time scale. This decrease in residence times is a result of the higher chance of falling out after each elevator trip, and the decreased time to pass from the midplane to the bottom boundary. It is also in this regime that we see agreement with the simplification made in Krueger [22], which assumed that settling rate follows Stokes law and that the mean lifetime is therefore proportional to $1/\mathrm{St}$ [shown by the reference slope in Fig. 5(a)]. This trend is perhaps more obvious in Fig. 5(b). It shows the mean residence time nondimensionalized by τ_w, which is the amount of time a given particle will take to settle in quiescent flow, defined as $\tau_w = 0.5L_z/(\tau_p g_p)$. In this context, it is evident that particles with $\mathrm{St} > 10^{-2}$ fall out at the rate predicted by Stokes law. Considering these results, it is evident that the transition that occurs around $\mathrm{St} = 10^{-4}$ in Fig. 5 is a result of the relative importance of the convective and settling time scales. For particles with $\mathrm{St} < 10^{-4}$, the vast majority of the residence time is a result of the elevator trips, which are a function of flow properties, and not their settling through the viscous boundary layer. When $\mathrm{St} > 10^{-4}$, the elevator trips make up an increasingly smaller percentage of the residence time, as reflected in the sharp increase in λ_f that also occurs around $\mathrm{St} = 10^{-4}$ [see Fig. 3(c)]. Once $\mathrm{St} > 10^{-2}$, particle residence times are almost entirely determined by the particle's Stokes drag [see Fig. 5(b)]. However, since St and V_s are still linked, it is still unclear whether this transition is associated with inertia (via St) or gravity (via V_s). In the next section, we will attempt to clarify those effects.

B. Fixed V_s, varying St

For this portion of the analysis, we choose three constant values of $V_s = [0.1, 1.0, 10]$. In the previous case, we were limited in how high of an St value we could consider because a corresponding V_s greater than 10^2 results in the particle falling out almost immediately. Here, however, we shift the range of values to $\mathrm{St} = [10^{-3}, 10^2]$ to encompass the transition between low to substantial inertial effects. Figure 6 shows the resulting residence PDFs for the full range of St along with some representative trajectories measured in the DNS.

As expected, it can be seen that for the same range of Stokes numbers, increasing the settling velocity decreases the residence time on average. Also of note is that by $V_s = 10$, none of the particles are able to complete an elevator trip as the flow is unable to carry them above the midplane due to their large settling velocity. It seems that in this regime, residence time is better parametrized by the particle's inertia and terminal speed as opposed to a convective scale. Of more interest, however, is how the residence times vary as a function of St given a constant V_s. These results are

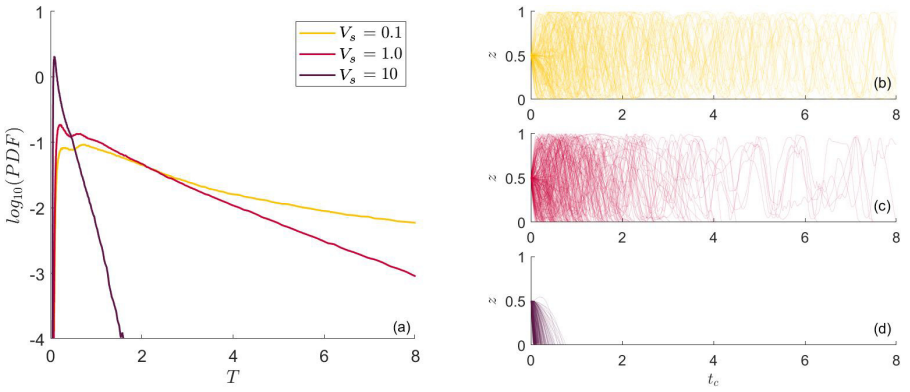

FIG. 6. DNS results from the constant V_s cases, for all particles over the range St $= [10^{-3}, 10^2]$: residence PDFs (a) and representative trajectories [(b)–(d)].

presented in Fig. 7, which shows that for low Stokes numbers ($<10^{-1}$), the residence time remains solely a function of V_s. As St increases, particle residence times initially decrease, but past St ≈ 10 they begin to increase again.

Figure 8 compares the PDFs for both the DNS and the model given the sample case of $V_s = 1.0$. We see that the model is again able to quantitatively replicate the PDF for the entire range of St, especially for the lower orders of magnitude. We believe that the discrepancy for the highest orders is a result of obtaining fewer data points for ρ_e due to the differences in the elevator trips that will be highlighted momentarily. In contrast to the case where St and V_s are linked, Fig. 9 shows that at a fixed settling velocity, St can change the distributions of ρ_e and ρ_b. For the largest particles (St > 10), we see an increase in the mean residence time in Fig. 7. The two main causes for this can be found in Fig. 9. First, we see that the time to complete an elevator trip (ρ_e) increases substantially, due to their delayed response to turbulence combined with the tendency to filter out small-scale motions. Secondly, the higher inertia also implies that they take longer to approach their terminal velocity, as evidenced by the increased time to travel from the midplane to the bottom boundary (ρ_b).

The other two model input parameters can be found in Fig. 10 for all three constant V_s values over the entire considered range of St. We can clearly see that λ_d is solely a function of V_s. We also notice that λ_f begins to increase once St is greater than 10^{-1}. This happens when particles are beginning to depart from streamlines, and are therefore flung towards the bottom boundary where

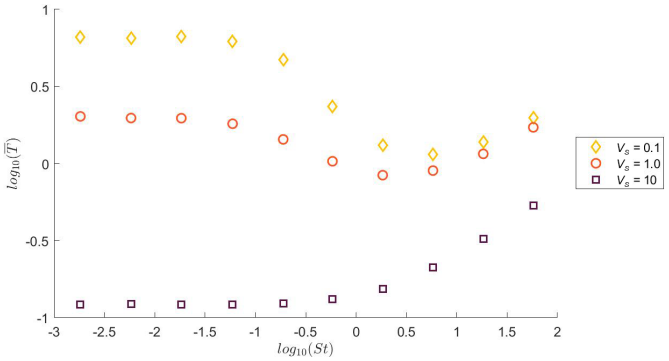

FIG. 7. Summary of the mean nondimensional residence times (T) over the range St $= [10^{-3}, 10^2]$ for each constant V_s.

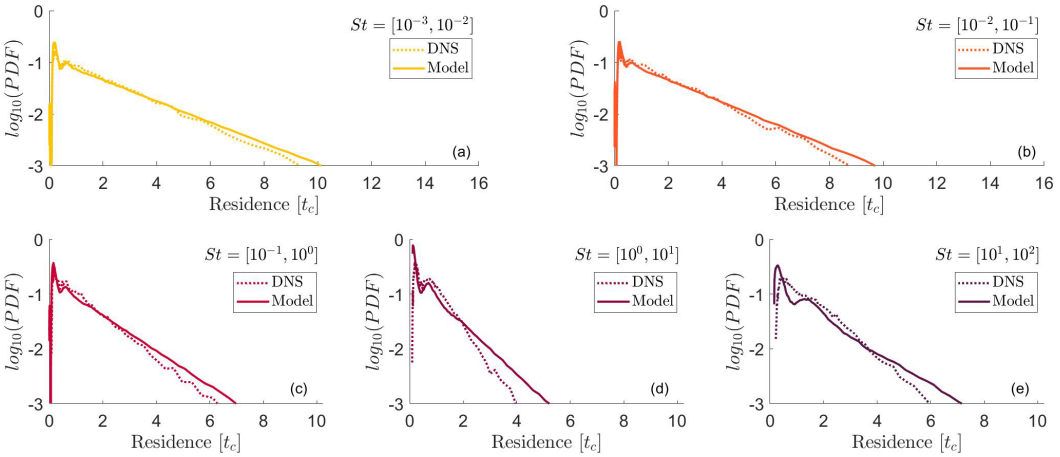

FIG. 8. The results of the fixed V_s, varying St cases as shown by the comparison of residence time distributions for the DNS and the model. For clarity, each order of magnitude of St is compared individually [(a)–(e)].

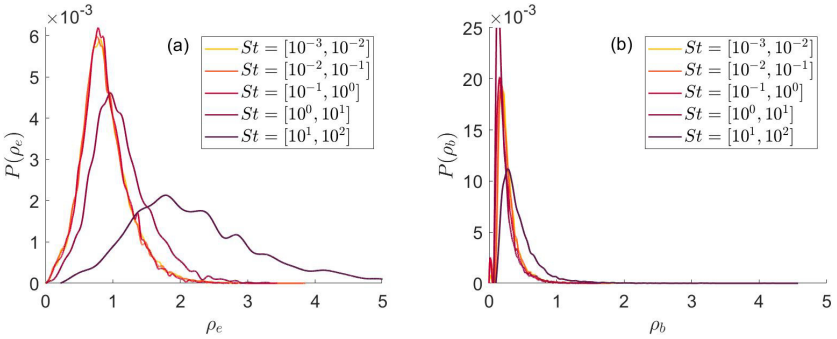

FIG. 9. For the sample case of $V_s = 1.0$, distributions for the time to complete and elevator trip, ρ_e (a), and the time to travel from the midplane to the bottom boundary, ρ_b (b).

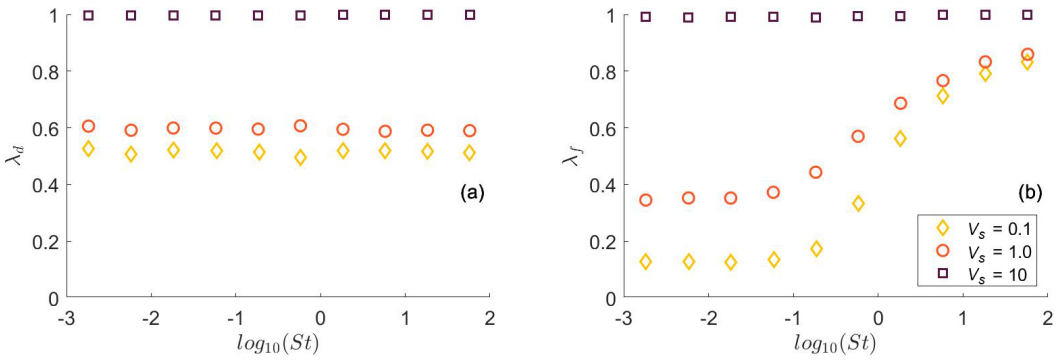

FIG. 10. For all three constant V_s cases, the percent chance of the particle initially having a downward velocity, λ_d (a), and the percent chance of falling out after each elevator trip, λ_f (b).

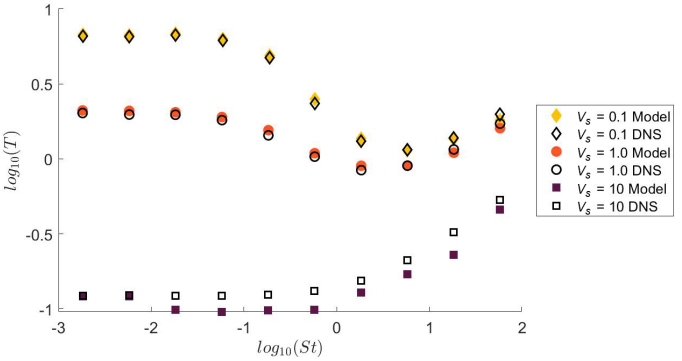

FIG. 11. Validation of the model results, shown by the mean nondimensional residence times (T) across the entire range of St for each constant V_s value.

they fall out. This would account for the initial dip in residence times that is seen in Fig. 7. At even higher St, the chance of falling out continues to approach 100% as St increases. This is because, as St continues to increase, the drag force on the particle becomes negligible compared with that produced by gravity, which pulls it towards the bottom boundary.

Figures 9 and 10 can be summarized in the following way. For small St ($<10^{-1}$), all particles are subject to the same turbulence-based convective time scale during their elevator trips, and the percent chance of falling out remains constant, leading to little change in their overall residence times. As St begins to increase ($10^{-1} < \mathrm{St} < 10^{1}$), elevator trips are still governed by the flow convective time scale, but the percent chance of falling out begins to increase due to the particles departing from streamlines, leading to a decrease in residence times. Once St becomes very large ($>10^{1}$), the particles have enough inertia to strongly resist the effects of the flow, and the elevator trips themselves become longer since they are experiencing a low-pass-filtered version of the surrounding turbulence. Even in the $V_s = 10$ case where particles rarely complete elevator trips, their high inertia prevents them from reaching their Stokes terminal velocity. This results in an increase in residence times, and we would expect the residence times to continue to increase along with St. Figure 11 shows how the model is able to match this behavior that was already demonstrated in the DNS results.

IV. DISCUSSION AND CONCLUSION

In this paper, we have proposed a stochastic model that reduces the complexities of particle-laden turbulent Rayleigh-Bénard flow to a simple conceptual picture. Motivated by the Pi Chamber experimental facility [4], we used one-way coupled DNS with Lagrangian particles to model their behavior and record statistics associated with their residence times. We focused in particular on the independent roles of St and V_s in dictating particle residence times in the flow.

In order to simplify the complex motion of the particles in the flow, we introduced the idea of an elevator trip which is the approximately sinusoidal motion generated by the convective Bénard cells. The four important statistics to describe this motion are the chance of a particle having an initial downward velocity, the time it takes to complete an elevator trip, the chance of falling out after an elevator trip, and the time it took to fall from the midplane to the bottom boundary. We have demonstrated that when these input statistics for the model are prescribed using DNS data, then the model predictions for the residence times accurately replicate the DNS results. That it should do so is not at all trivial given the complexity of particle motion in turbulent Rayleigh-Bénard flow, and the simplicity of the approximations underlying the model. This test accomplishes two things. First, it demonstrates that with perfect knowledge of the inputs, the stochastic model provides a very good approximation of both the mean and full distribution of residence times. Secondly, it shows that this

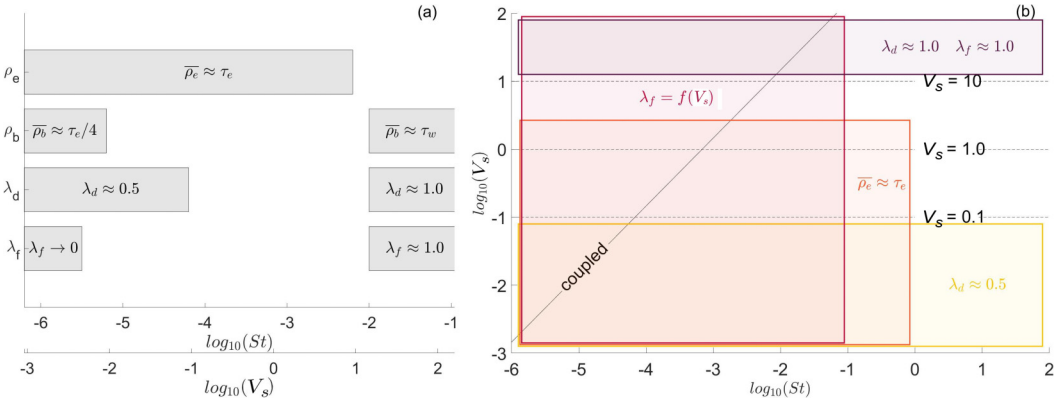

FIG. 12. Summary of the potential simplifying assumptions in various regimes of St and V_s for both the coupled (a) and uncoupled (b) case.

simple conceptual framework provides insight into the physical phenomena governing the particle residence times in this system.

When St and V_s are coupled, as they would in experimental conditions, we saw that the amount of time to complete an elevator trip remained constant, but as St increased more particles had an initial downward velocity, and they were more likely to fall out after a given elevator trip. This unsurprisingly results in larger particles having shorter residence times. To clarify the independent roles of St and V_s, we chose three constant, representative values of V_s and varied St for each to isolate the effects of inertia. In these runs, we saw that for small St, residence times are solely a function of V_s since the lifetime is ultimately dictated by the particles settling through the boundary layer, which is not aided by particle inertia when St is small. However, as St begins to increase, so does the chance of falling out after each elevator trip, leading to an initial decrease in residence times. This corresponds to particles departing from streamlines and being flung out of the turbulent core of the domain. For the largest St, the increased inertia leads to longer elevator trips and slow relaxation to their Stokes terminal velocity, resulting in a reversion towards longer residence times. Using this knowledge, we can look at our coupled St and V_s results in a new light. For particles with $\mathrm{St} < 10^{-4}$, motion is dominated by the flow properties that determine the number of elevator trips. In contrast, the residence time of particles with $\mathrm{St} < 10^{-4}$ is increasingly more dependent on the particle's settling rate in quiescent flow.

In the end, we demonstrated that the simple conceptual framework underlying the stochastic model provides a helpful way to understand the behavior of the particles in the flow, and if the input statistics are perfectly described, then it also provides accurate approximations for both the mean residence times and their complete probability distributions. At the moment, the model relies on DNS data to prescribe the input statistics. In future work, a key point will be to develop models for the four statistical inputs themselves, so that the stochastic model for the particle residence times is fully closed. From the results we can already see that the convective time scale (t_c) is helpful in predicting the average time it takes to complete an elevator trip. While it is beyond the scope of this paper, there is promise in finding similar relationships for the other inputs.

To support this effort, Fig. 12 provides a summary of the simplifying assumptions that can be made in various regimes. Figure 12(a) summarizes the coupled results, in which the limit cases are apparent. For very small particles ($\mathrm{St} \lesssim 10^{-6}$) that nearly behave like fluid tracers, the average elevator trip is approximately the eddy turnover time ($\overline{\rho_e} \approx \tau_e$), the particles are carried to the bottom boundary by the flow ($\overline{\rho_b} \approx \tau_e/4$), there is an equal chance of an initial upward or downward velocity when initialized at the midplane ($\lambda_d \approx 0.5$), and the chance of falling out after each elevator trip tends towards zero ($\lambda_f \to 0$). For the largest particles ($\mathrm{St} \gtrsim 10^{-1}$), the particles are driven to

the bottom boundary by their settling velocity ($\overline{\rho_b} \approx \tau_w$), and particles nearly always have an initial downward velocity ($\lambda_d \approx 1.0$) and fall out of the flow at the first opportunity ($\lambda_f \approx 1.0$).

Figure 12(b) shows the simplifying assumptions that can be made in light of the uncoupled case. Over the entire range of St, when $V_s \leqslant 0.1$ the mean vertical fluid velocity determines the chance of an initial downward velocity ($\lambda_d \approx 0.5$), and when $V_s \geqslant 10$, the particles nearly always have an initial downward velocity ($\lambda_d \approx 1.0$) and fall out of the flow at the first opportunity ($\lambda_f \approx 1.0$). We also observed that the chance of falling out after each elevator trip was solely a function of the settling velocity [$\lambda_f = f(V_s)$] until $\mathrm{St} \gtrsim 10^{-1}$, at which point inertia begins to play a role. The assumption that the mean time to complete an elevator trip is approximately equal to the eddy turnover time (τ_e) holds as long as $\mathrm{St} \lesssim 1$ and $V_s \lesssim 1$, beyond which the inertia and gravitational settling become a contributing factor.

This demonstrates that, in certain regimes, many of the components of the model proposed here can be simplified, reducing the dependence on the DNS. For instance, the salt aerosols often injected into the Pi Chamber are on the order of $\mathrm{St} \sim O(10^{-6})$, which allows us to make assumptions about all four input parameters. It is also worth noting that since the length of each elevator trip is decided independently of the others, we are free to vary particle properties after each trip. If the particle size were to be updated based on the relative humidity encountered, this model could potentially be extended to evaporating particles. In conjunction with a number of the potential simplifying assumptions, this could provide a model with even more direct applications to the Pi Chamber.

ACKNOWLEDGMENTS

This research was supported by NSF Grant No. AGS-2227012. The authors gratefully acknowledge computing support from the Notre Dame Center for Research Computing.

[1] H. F. Schwaiger, R. P. Denlinger, and L. G. Mastin, Ash3d: A finite-volume, conservative numerical model for ash transport and tephra deposition, J. Geophys. Res.: Solid Earth **117**, B04204 (2012).

[2] J. Ruiz, D. Macías, and F. Peters, Turbulence increases the average settling velocity of phytoplankton cells, Proc. Natl. Acad. Sci. USA **101**, 17720 (2004).

[3] V. Patočka, E. Calzavarini, and N. Tosi, Settling of inertial particles in turbulent Rayleigh-Bénard convection, Phys. Rev. Fluids **5**, 114304 (2020).

[4] K. Chang, J. Bench, M. Brege, W. Cantrell, K. Chandrakar, D. Ciochetto, C. Mazzoleni, L. R. Mazzoleni, D. Niedermeier, and R. A. Shaw, A laboratory facility to study gas-aerosol cloud interactions in a turbulent environment: The Π chamber, Bull. Am. Meteorol. Soc. **97**, 2343 (2016).

[5] K. K. Chandrakar, W. Cantrell, S. Krueger, R. A. Shaw, and S. Wunsch, Supersaturation fluctuations in moist turbulent Rayleigh-Bénard convection: A two-scalar transport problem, J. Fluid Mech. **884**, A19 (2020).

[6] P. Oresta, F. Fornarelli, and A. Prosperetti, Multiphase Rayleigh-Bénard convection, Mech. Eng. Rev. **1**, FE0003 (2014).

[7] R. Lakkaraju, R. J. Stevens, P. Oresta, R. Verzicco, D. Lohse, and A. Prosperetti, Heat transport in bubbling turbulent convection, Proc. Natl. Acad. Sci. USA **110**, 9237 (2013).

[8] J. W. Scanlon and L. A. Segel, Some effects of suspended particles on the onset of Bénard convection, Phys. Fluids **16**, 1573 (1973).

[9] P. Oresta and A. Prosperetti, Effects of particle settling on Rayleigh-Bénard convection, Phys. Rev. E **87**, 063014 (2013).

[10] W. Yang, Y. Z. Zhang, B. F. Wang, Y. Dong, and Q. Zhou, Dynamic coupling between carrier and dispersed phases in Rayleigh-Bénard convection laden with inertial isothermal particles, J. Fluid Mech. **930**, A24 (2022).

[11] L. Brandt and F. Coletti, Annual review of fluid mechanics particle-laden turbulence: Progress and perspectives, Annu. Rev. Fluid Mech. **54**, 159 (2022).

[12] H. J. Park, K. O'Keefe, and D. H. Richter, Rayleigh-Bénard turbulence modified by two-way coupled inertial, nonisothermal particles, Phys. Rev. Fluids **3**, 034307 (2018).
[13] M. R. Maxey, The gravitational settling of aerosol particles in homogeneous turbulence and random flow fields, J. Fluid Mech. **174**, 441 (1987).
[14] A. Aliseda, A. Cartellier, F. Hainaux, and J. C. Lasheras, Effect of preferential concentration on the settling velocity of heavy particles in homogeneous isotropic turbulence, J. Fluid Mech. **468**, 77 (2002).
[15] L.-P. Wang and M. R. Maxey, Settling velocity and concentration distribution of heavy particles in homogeneous isotropic turbulence, J. Fluid Mech. **256**, 27 (1993).
[16] J. Tom and A. D. Bragg, Multiscale preferential sweeping of particles settling in turbulence, J. Fluid Mech. **871**, 244 (2019).
[17] B. Rosa, H. Parishani, O. Ayala, and L. P. Wang, Settling velocity of small inertial particles in homogeneous isotropic turbulence from high-resolution DNS, Int. J. Multiphase Flow **83**, 217 (2016).
[18] G. H. Good, P. J. Ireland, G. P. Bewley, E. Bodenschatz, L. R. Collins, and Z. Warhaft, Settling regimes of inertial particles in isotropic turbulence, J. Fluid Mech. **759**, R3 (2014).
[19] A. D. Bragg, D. H. Richter, and G. Wang, Mechanisms governing the settling velocities and spatial distributions of inertial particles in wall-bounded turbulence, Phys. Rev. Fluids **6**, 064302 (2021).
[20] A. D. Bragg, D. H. Richter, and G. Wang, Settling strongly modifies particle concentrations in wall-bounded turbulent flows even when the settling parameter is asymptotically small, Phys. Rev. Fluids **6**, 124301 (2021).
[21] M. W. Reeks, The transport of discrete particles in inhomogeneous turbulence, J. Aerosol Sci. **14**, 729 (1983).
[22] S. K. Krueger, Technical note: Equilibrium droplet size distributions in a turbulent cloud chamber with uniform supersaturation, Atmos. Chem. Phys. **20**, 7895 (2020).
[23] I. Saito, T. Gotoh, and T. Watanabe, Broadening of cloud droplet size distributions by condensation in turbulence, J. Meteorol. Soc. Jpn. **97**, 867 (2019).
[24] R. Paoli and K. Shariff, Turbulent condensation of droplets: Direct simulation and a stochastic model, J. Atmos. Sci. **66**, 723 (2009).
[25] K. Chandrakar and F. Yang, Droplet size distributions in turbulent clouds: Experimental evaluation of theoretical distributions, Q. J. R. Meteorolog. Soc. **146**, 483 (2019).
[26] T. MacMillan, R. A. Shaw, W. H. Cantrell, and D. H. Richter, Direct numerical simulation of turbulence and microphysics in the Pi chamber, Phys. Rev. Fluids **7**, 020501 (2022).
[27] D. H. Richter, T. MacMillan, and C. Wainwright, A Lagrangian cloud model for the study of marine fog, Boundary Layer Meteorol.**181**, 523 (2021).
[28] B. Helgans and D. H. Richter, Turbulent latent and sensible heat flux in the presence of evaporative droplets, Int. J. Multiphase Flow **78**, 1 (2016).
[29] M. R. Maxey and J. J. Riley, Equation of motion for a small rigid sphere in a nonuniform flow, Phys. Fluids **26**, 883 (1983).
[30] P. J. Sakievich, Y. T. Peet, and R. J. Adrian, Large-scale thermal motions of turbulent rayleigh–Bénard convection in a wide aspect-ratio cylindrical domain, Int. J. Heat Fluid Flow **61**, 183 (2016).
[31] P. J. Sakievich, Y. T. Peet, and R. J. Adrian, Temporal dynamics of large-scale structures for turbulent Rayleigh-Bénard convection in a moderate aspect-ratio cylinder, J. Fluid Mech. **901**, A31 (2020).
[32] E. Bodenschatz, W. Pesch, and G. Ahlers, Recent developments in Rayleigh-Bénard convection, Annu. Rev. Fluid Mech. **32**, 709 (2000).
[33] H. Rouse, Modern conceptions of the mechanics of fluid turbulence, Am. Soc. Civ. Eng. Trans. **102**, 463 (1937).